Predicting the rotational constraint in stratified, compressible convection

Evan H. Anders,[1,2] Cathryn M. Manduca,[2] Benjamin P. Brown,[1,2] and Jeffrey S. Oishi[3]

[1]*Dept. Astrophysical & Planetary Sciences, University of Colorado – Boulder, Boulder, CO 80309, USA*
[2]*Laboratory for Atmospheric and Space Physics, Boulder, CO 80303, USA*
[3]*Department of Physics and Astronomy, Bates College, Lewiston, ME 04240, USA*

ABSTRACT

Here we study numerical simulations of stratified, compressible convection in a rotational f-plane geometry. We discuss how the rotational constraint, measured by the Rossby number (Ro), can vary as a function of the convective driving, measured by the Rayleigh number (Ra). We define a relationship between Ra and the Taylor number (Ta) which we call the Predictive Rossby Number, $\mathcal{P}_{\mathrm{Ro}} = $ Ra / $\mathrm{Ta}^{3/4}$, and we find that the Ro remains roughly constant across orders of magnitude of Ra when $\mathcal{P}_{\mathrm{Ro}}$ is fixed.

1. INTRODUCTION

Convective flows in stars and planets are influenced by rotation. Rotating convection has been studied in great detail in recent decades in both laboratory and numerical settings. The properties of convection in the regime in which rotational forces are insignificant are now well understood (King et al. 2009; Zhong et al. 2009; **?**). Boussinesq convective theory is also robust in the rapidly rotating regime (Julien et al. 2012; Stellmach et al. 2014; **?**). We are not, however, aware of any well-developed procedure for specifying the degree of rotational constraint in a convective experiment *a priori*. Rather, the rotational constraint, measured by the evolved Rossby number (Ro, the ratio of advective dynamics to rotational constraint), is a complex combination of input parameters, such as convective driving and the magnitude of the rotation vector.

A vast number of studies of rotating convection have been conducted in the astrophysical context. Often these studies focus on questions inspired by the solar dynamo (Glatzmaier & Gilman 1982; Busse 2002; Brown et al. 2008, 2010, 2011; Augustson et al. 2012; Guerrero et al. 2013; Käpylä et al. 2014). Even when these

simulations appear to be rotating at a rate similar to the Sun, they can produce vastly different dynamics (such as anti-solar differential rotation). These strange results may be the result of these systems having different evolved values of the Rossby number than the Sun. Recent simulations and experiments are predicting that the Rossby number of the deep interior of the Sun is low, and that this drastically affects the behavior of the dynamics of the solar convection zone (Featherstone & Hindman 2016; Greer et al. 2016).

In addition to it being very important to study the correct Rossby number regime in solar convection studies, it also seems to be very important in studies of planetary dynamos. For example, the balance between Lorentz forces and rotational forces likely creates the observed differences between ice giant and gas giant dynamos in our solar system (Soderlund et al. 2015). Furthermore, Aurnou & King (2017) suggest that many studies in planetary systems have likely over-emphasized the importance of magnetism compared to rotation.

It is clear that in studying astrophysical objects, the experimenter must study the proper Rossby number regime, and thus the proper degree of rotational constraint. In this work, our goal is to find a way of specifying the Rossby number of convection in a simplified system through changing the input parameters. In Anders & Brown (2017) (hereafter AB17), we studied non-rotating, hydrodynamic, compressible convec-
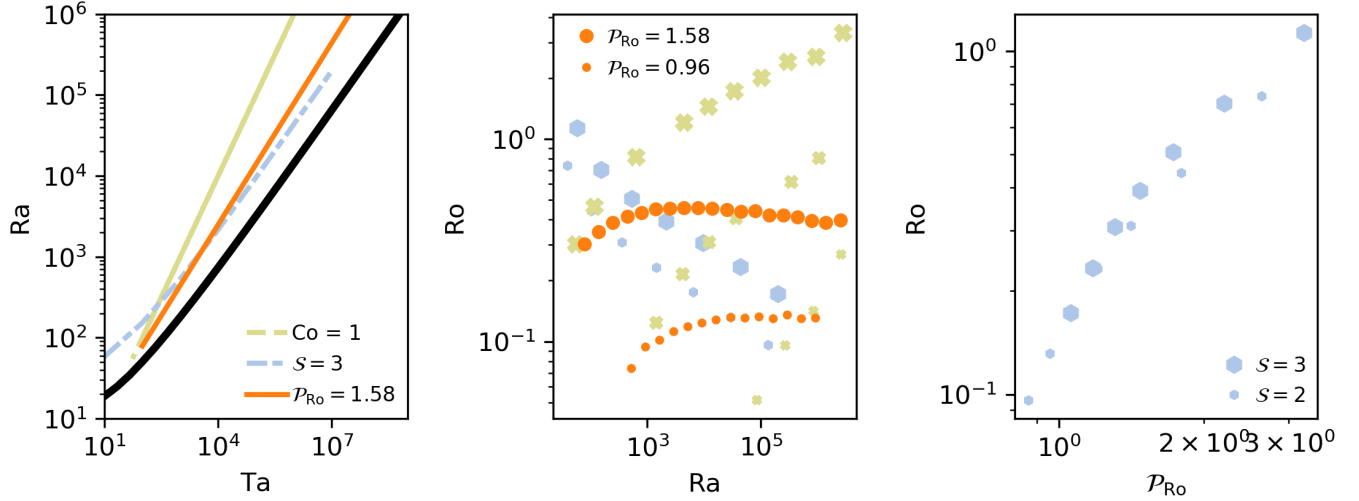
Corresponding author: Evan H. Anders
evan.anders@colorado.edu

Figure 1. (a) The critical Rayleigh number, as a function of the Taylor number, is plotted as a solid black line. Paths of constant Convective Rossby Number (red dashed line), constant supercriticality (orange dashed line), and $\mathcal{P}_{\mathrm{Ro}}$ (blue solid line) are shown through parameter space. (b) Evolved Ro is plotted vs. Ra along multiple constant $\mathcal{P}_{\mathrm{Ro}}$ paths and the constant Co and $\mathcal{S}$ path shown in (a). After a sharp increase at low Ta, the evolved Rossby number flattens out and stays nearly constant across orders of magnitude of Ta. (c) At low Ro, we find that Ro $\propto \mathcal{P}_{\mathrm{Ro}}{}^{X}$.

tion in polytropic atmospheres. In this work, we extend the study of AB17 to rotationally-influenced, f-plane atmospheres, as have been previously studied by e.g., Brummell et al. (1996, 1998); Calkins et al. (2015). Our goal is to determine how the input parameters which we studied previously (which control the Mach number and Reynolds number of the evolved flows) couple with a new input parameter, the Taylor number (Ta, Julien et al. (1996)), which sets the magnitude of the rotational vector.

In section 2, we describe our atmosphere, numerical experiment, and paths through parameter space. In section 3, we present the results of our experiments and in section 4 we offer concluding remarks.

2. EXPERIMENT

We study fully compressible, stratified convection under precisely the same atmospheric model as we previously did in AB17, but here we have included rotation. We study polytropic atmospheres with $n_\rho = 3$ density scale heights and a superadiabatic excess of $\epsilon = 10^{-4}$ such that flows are at low Mach number. As in previous work (Julien et al. 1996; Brummell et al. 1996), we study a domain in which the gravity, $\boldsymbol{g} = -g\hat{z}$, and rotational vector, $\boldsymbol{\Omega} = \Omega\hat{z}$, are antiparallel.

We evolve the velocity ($\boldsymbol{u}$), temperature (T), and log density ($\ln\rho$) according to the Fully Compressible Navier-Stokes equations in the same form presented in AB17, with the addition of the Coriolis term, $2\boldsymbol{\Omega} \times \boldsymbol{u}$, to the left-hand side of the momentum equation.

The kinematic viscosity (ν), thermal diffusivity (χ), and strength of rotation (Ω) are set at the top of the domain by the Rayleigh number (Ra), Prandtl number (Pr), and Taylor number (Ta),

$$\mathrm{Ra} = \frac{gL_z^3 \Delta S/c_P}{\nu\chi}, \ \ \mathrm{Pr} = \frac{\nu}{\chi}, \ \ \mathrm{Ta} = \left(\frac{2\Omega L_z^2}{\nu}\right)^2, \quad (1)$$

where L_z is the depth of the domain, $\Delta S = \epsilon n_\rho/m$ is the specific entropy difference between $z = 0$ and $z = L_z$, and the specific heat at constant pressure is c_P. Throughout this work we set Pr = 1.

As Ta increases, the critical value of Ra at which convection onsets, $\mathrm{Ra_{crit}}$, also increases (see the black line in Fig. 1a). The linked nature of these crucial control parameters makes it difficult to predict the rotational constraint of the evolved fluid flows for a given set of input parameters. In this work, we will explore three paths through Ra-Ta space:

$$\mathrm{Ra} = \begin{cases} \mathcal{S}\,\mathrm{Ra_{crit}(Ta)}, & \text{(I)} \\ \mathrm{Co}^2\mathrm{Pr\,Ta}, & \text{(II)} \\ \mathcal{P}_{\mathrm{Ro}}{}^2\mathrm{Pr\,Ta}^{3/4} & \text{(III)}. \end{cases} \quad (2)$$

Paths on constraint I are at constant supercriticality, $\mathcal{S}$ (orange dash-dot line in Fig. 1a). Paths on constraint II are at a constant value of the classic "Convective Rossby number" (Co), which has been used frequently over the past two decades, and is intended to predict the rotational constraint of the evolved solution (red line in Fig. 1a; Julien et al. (1996); Brummell et al. (1996)). Paths
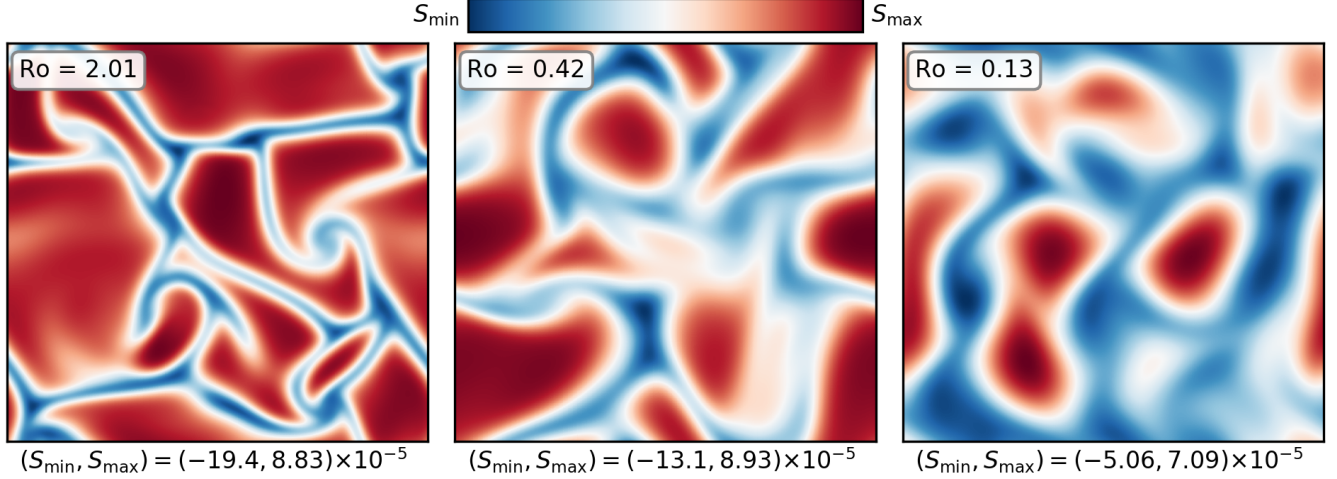
Figure 2. A horizontal slice of the evolved entropy field is plotted at $z = 0.95L_z$ for select simulations. The mean value of entropy at this height has been removed in all cases. All runs displayed here have an evolved volume-averaged Ro $\sim$ 200. As Ro decreases O(1) on the left to O(0.1) on the right, and thus the rotational constraint on the flow increases, significant changes in flow morphology are observed. At Ro = 2.01, convective dynamics are not hugely dissimilar from the non-rotating case where there are large upflows and narrow, fast downflow lanes (see e.g., AB17). As the rotational constraint increases, the granular convective pattern gives way to vortical columns, as seen at Ro = 0.13.

on constraint III set constant a ratio which we call the "Predictive Rossby Number" ($\mathcal{P}_{\mathrm{Ro}}$). These paths follow contours of $\mathrm{Ta}^{3/4}$, and to our knowledge have not been well-explored in the literature (blue solid line in Fig. 1a).

In this work, our goal is to study the magnitude of the rotational constraint along each path defined in Eqn. 2. We will quantify rotational constraint using the Rossby number,

$$\mathrm{Ro} = \frac{|\nabla \times \boldsymbol{u}|}{2\Omega}. \tag{3}$$

As Ta increases, the wavenumber of convective onset, k_{crit}, also increases. We study 3D cartesian convective domains with horizontal extents of $x, y = [0, 4(2\pi/k_{\mathrm{crit}})]$. We evolve our simulations using the Dedalus[1] pseudospectral framework, and our numerical methods are identical to those presented in AB17.

3. RESULTS & DISCUSSION

In Fig. 1a, we display the value of the critical Rayleigh number ($\mathrm{Ra}_{\mathrm{crit}}$) as a function of the Taylor number (Ta). We found these critical values through the use of a linear instability analysis. We plot a sample path for each criterion in Eqn. 2 through this parameter space. In Fig. 1b, we show that along paths of constant $\mathcal{S}$, Ro decreases as a function of Ra and Ta. Along paths of constant Co, Ro increases with increasing Ra and Ta. However, along paths of constant $\mathcal{P}_{\mathrm{Ro}}$, after an increase at low Ra, the

evolved value of Ro levels off and stays roughly constant as a function of Ra. Holding $\mathcal{P}_{\mathrm{Ro}}$ constant seems to predict Ro relatively well from our experimental trials here, particularly at low Ro. In Fig. 1c, we show how the Ro varies as a function of $\mathcal{P}_{\mathrm{Ro}}$ at constant supercriticality. We expect the scaling law for Ro ≤ 0.4 to hold up to low Ro, and the leveling off seen at higher Ro and higher $\mathcal{P}_{\mathrm{Ro}}$ is likely influenced by the curvature of the supercriticality curve at low Ra and Ta (see Fig. 1a).

In Fig. 2, we show sample snapshots of the evolved entropy field near the top of the domain. The cases displayed have evolved Ro spanning roughly an order of magnitude. As we study the increasingly rotationally constrained regime, we see the classic granular structure of convection (see e.g., Fig. 2 in AB17) give way to vortical columns of convection, as seen in rapidly rotating Rayleigh-Bénard convection (Stellmach et al. 2014). All cases displayed in Fig. 2 have an evolved volume-averaged Re of roughly 200.

We define the Nusselt number (Nu, which quantifies heat transport in a convective solution) as we did previously in AB17. In Fig. 3a, we show the scaling of Nu as a function of Ra at fixed $\mathcal{P}_{\mathrm{Ro}}$. We find that when $\mathcal{P}_{\mathrm{Ro}}$ is held constant and Ra is increased, we find a scaling of Nu $\propto \mathrm{Ra}^{0.27}$, which is reminiscent of classical scaling laws in non-rotating theory, and suggests that changes in heat transport along these paths are boundary driven. Furthermore, in Fig. 3b, we plot the RMS Reynold's number (Re $= |u|L_z/\nu$) as a function of Ra,
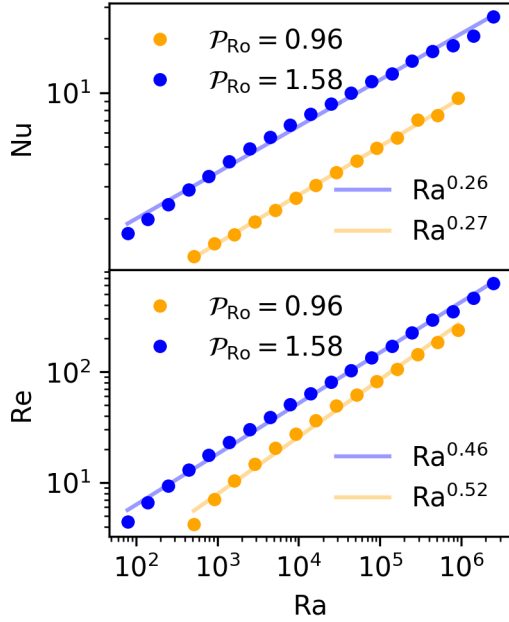
---

[1] http://dedalus-project.org/

Figure 3. (a) Evolved Nu vs. Ra along constant $\mathcal{P}_{\mathrm{Ro}}$ paths. A scaling law of $\mathrm{Nu} \propto \mathrm{Ra}^{0.27}$ is observed, which is very similar to classic scaling laws. (b) Evolved Re vs. Ra along constant $\mathcal{P}_{\mathrm{Ro}}$ paths. A classic scaling law of $\mathrm{Re} \propto \mathrm{Ra}^{1/2}$ is observed. The similarity between these laws and classical laws in Rayleigh-Bénard convection suggests that at fixed $\mathcal{P}_{\mathrm{Ro}}$, varying Ra affects the evolved dynamics in a manner similar to a nonrotating fluid.

and find that $\mathrm{Re} \propto \mathrm{Ra}^{1/2}$, which is precisely the scaling we found in the non-rotating regime in AB17.

In Fig. 4, we show time- and horizontally-averaged profiles of the rossby number and the entropy gradient. As Ra increases at a constant value of $\mathcal{P}_{\mathrm{Ro}}$, both the entropy and rotational boundary layers shrink. We measure the upper boundary layer thicknesses of both profiles. We measure the boundary layer thickness of the Rossby number as the distance from the upper boundary to the point at which Ro is maximized. We measure the boundary layer thickness of the entropy profile by

fitting a line to the upper 10 points in the domain, and assuming that the boundary layer extends to the point at which that line crosses through zero. We plot $\delta_S/\delta_{\mathrm{Ro}}$ as a function of Ra for our $\mathcal{P}_{\mathrm{Ro}}$ paths in Fig. 4b. We find that the ratio of these boundary layers is relatively constant as a fucntion of Ra, which implies that the rotational constraint across Ra is roughly constant. [NOTE: NEED TO TALK ABOUT MAGNITUDE OF RO IN BOUNDARY LAYER]

4. DISCUSSION

In this letter, we studied rotating, stratified, compressible convection at low Mach number. We studied traditional paths through Ra-Ta space, as well as a new path, in which the Predictive Rossby number, $\mathcal{P}_{\mathrm{Ro}}$, is held constant, and $\mathrm{Ra} = \mathcal{P}_{\mathrm{Ro}} \, \mathrm{Ta}^{3/4}$. Along these paths, we find that the evolved rotational constraint, as measured by the Rossby number (Ro), is roughly constant as Ra increases. Furthermore, the heat transport, measured by the Nusselt number (Nu), and the level of turbulence, as measured by the Reynolds number (Re), vary according to traditional scaling laws as Ra increases. Together, these phenomena suggest that experimenters in stratified convection can specify the degree of rotational constraint in their evolved solutions by choosing $\mathcal{P}_{\mathrm{Ro}}$, and then increase Ra in a manner analogous to unrotating convection (e.g., AB17) to increase the efficiency and turbulent nature of the convective dynamics in question.

4.1. acknowledgements

REFERENCES

Anders, E. H., & Brown, B. P. 2017, Physical Review Fluids, 2, 083501

Augustson, K. C., Brown, B. P., Brun, A. S., Miesch, M. S., & Toomre, J. 2012, ApJ, 756, 169

Aurnou, J. M., & King, E. M. 2017, Proceedings of the Royal Society of London Series A, 473, 20160731

Brown, B. P., Browning, M. K., Brun, A. S., Miesch, M. S., & Toomre, J. 2008, ApJ, 689, 1354

—. 2010, ApJ, 711, 424

Brown, B. P., Miesch, M. S., Browning, M. K., Brun, A. S., & Toomre, J. 2011, ApJ, 731, 69

Brummell, N. H., Hurlburt, N. E., & Toomre, J. 1996, ApJ, 473, 494

—. 1998, ApJ, 493, 955

Busse, F. H. 2002, Physics of Fluids, 14, 1301

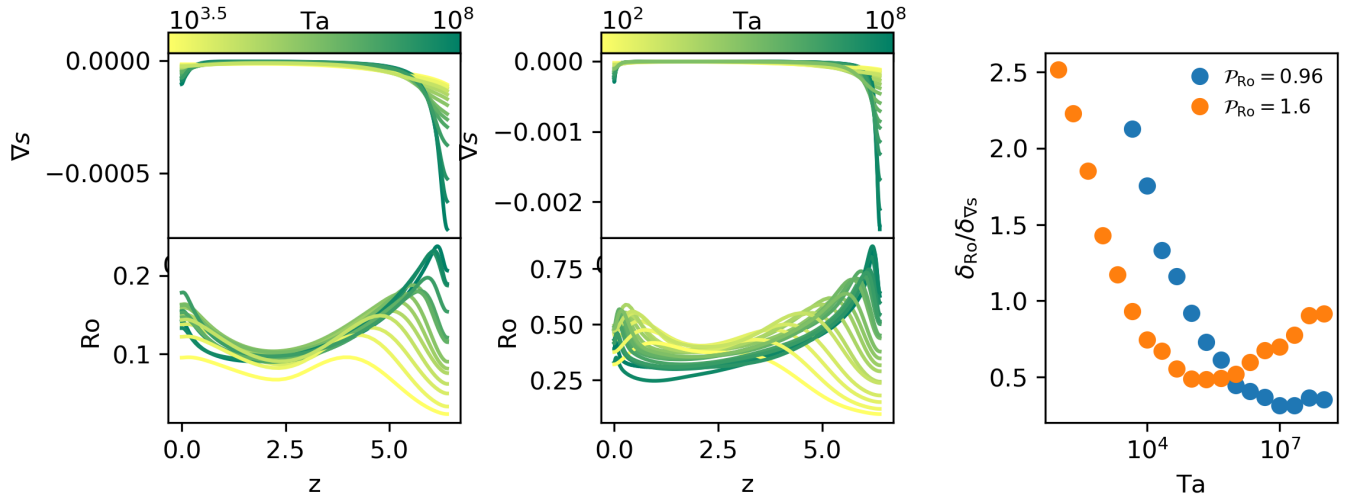Calkins, M. A., Julien, K., & Marti, P. 2015, Geophysical and Astrophysical Fluid Dynamics, 109, 422

Figure 4. (a) Horizontally-averaged profiles of the Rossby number are shown vs. z for a constant $\mathcal{P}_{\mathrm{Ro}}$ = X. (b) Horizontally-averaged profiles of the entropy gradient are shown vs. z for a constant $\mathcal{P}_{\mathrm{Ro}}$ = X. (c) Vorticity boundary layer thickness normalized by entropy boundary layer thickness as a function of Ta/Ta_crit for multiple $\mathcal{P}_{\mathrm{Ro}}$ paths. When this measure is $\gg 1$, we expect the flows to be buoyancy dominated, when it is $\ll 1$, we expect the flows to be rotationally dominated, and when it is ~ 1, we anticipate that both effects are very important.

Featherstone, N. A., & Hindman, B. W. 2016, ApJ, 830, L15

Glatzmaier, G. A., & Gilman, P. A. 1982, ApJ, 256, 316

Greer, B. J., Hindman, B. W., Featherstone, N. A., & Toomre, J. 2015, ApJL, 803, L17

Greer, B. J., Hindman, B. W., & Toomre, J. 2016, ApJ, 824, 4

Guerrero, G., Smolarkiewicz, P. K., Kosovichev, A. G., & Mansour, N. N. 2013, ApJ, 779, 176

Hanasoge, S. M., Duvall, T. L., & Sreenivasan, K. R. 2012, Proceedings of the National Academy of Science, 109, 11928

Julien, K., Knobloch, E., Rubio, A. M., & Vasil, G. M. 2012, Physical Review Letters, 109, 254503

Julien, K., Legg, S., McWilliams, J., & Werne, J. 1996, Journal of Fluid Mechanics, 322, 243

Käpylä, P. J., Käpylä, M. J., & Brandenburg, A. 2014, A&A, 570, A43

King, E. M., Stellmach, S., Noir, J., Hansen, U., & Aurnou, J. M. 2009, Nature, 457, 301

Soderlund, K. M., Sheyko, A., King, E. M., & Aurnou, J. M. 2015, Progress in Earth and Planetary Science, 2, 24

Stellmach, S., Lischper, M., Julien, K., et al. 2014, PhRvL, 113, 254501

Stevens, R. J. A. M., Zhong, J.-Q., Clercx, H. J. H., Ahlers, G., & Lohse, D. 2009, PhRvL, 103, 024503

Zhong, J.-Q., Stevens, R. J. A. M., Clercx, H. J. H., et al. 2009, Physical Review Letters, 102, 044502